An Organometallic Ir(III) Molecular Probe for Imaging Microtubules in Fluorescence and Electron Microscopy

Xiaohe Tian,[ab] Cesare De Pace,[cde] Lorena Ruiz-Perez,[cde] Bo Chen,[f] Rina Su,[a] Mingzhu Zhang,[b] Ruilong Zhang,[b] Qiong Zhang,[b] Qin Wang,[g] Hongping Zhou,[b] Jieying Wu,[b] Giuseppe Battaglia,[cde] Zhongping Zhang,[bh*] Yupeng Tian[b*]*

[a]School of Life Science, Anhui University, Hefei 230039, P. R. China. [b]Department of Chemistry, Key Laboratory of Functional Inorganic Material Chemistry of Anhui Province, Anhui University, Hefei 230039, P. R. China. [c]Department of Chemistry, University College London, London, WC1H 0AJ, UK. [d]Department of Chemical Engineering, University College London, London, WC1H 0AJ, UK. [e]TheEPSRC/Jeol Centre of Liquid Electron Microscopy, University College London, London, WC1H 0AJ, UK. [f] School of Materials Science and Engineering, Tongji University, Shanghai, 201804, P. R. China. [g] Biotechnology Centre, Anhui Agriculture University, Hefei, 230036, P. R. China [h]CAS Center for Excellence in Nanoscience, Institute of Intelligent Machines, Chinese Academy of Sciences, Hefei, Anhui 230031, P. R. China

Abstract:

Microtubules are a critical component of the cell cytoskeleton and an important actor in cell mitosis and adhesion. Yet their imaging has been limited by the lack of effective probes. Fluorescent imaging can be performed using either taxol derivates, immunoglobins, or genetically encoded fluorescent proteins. These approaches however tend to hinder microtubulin functionality and they do not bestow any contrast in electron microscopy. Here we present a cyclometalated Iridium(III) complex that bind to microtubulin and allow both fluorescent and electron microscopy imaging. The complex displays a 'light switch' phenomena coupled with strong luminescence intensity upon tubulin protein binding without interfering into cell proliferation. Furthermore, the application of super resolution imaging of microtubule ultrastructure within brain neuron network under stimulated emission depletion (STED) microscopy was successfully demonstrated. More importantly, the **Ir-Tub** showed its capability to display microtubule structure under protein monomeric level by means of energy filtered transmission electron microscopy (EF-TEM). This innovative complex sheds light on the visualization and modeling of precise microtubule structure, aiding a much better understanding of correlated cellular mechanisms and ultimately associated diseases.

Introduction:

Microtubules are one of the major components of cytoskeleton in all eukaryotic cells and are made by the self-assembly of tubulins. These are both α- and β- dimers and its polymerisation is controlled through GTP (Guanosine-5'-triphosphate) binding.[1, 2] Microtubules serve as scaffold for most organelles as well as paths for kinesin motors to facilitate transport within the cells. Microtubules regulate clathrin-mediated endocytosis,[3] and enable DNA segregation and consequent cell division dynamics during mitosis from prometaphase to telophase.[4] This latter function has made tubulin a very important anticancer agent with several drugs being designed to bind and inhibit its polymerisation including nocodozale and taxols.[5] It appears evident that the designs of probes that target selectively tubulin, without affecting its activity are critical for shedding light on related intracellular activities. The most typical probes used for fluorescence imaging of microtubules involve antibodies hence the use is limited to pre-fixed cells and tissues,[6, 7] unspecific staining with other cytoskeleton species (e.g. actin), as well as ~20-30nm resolution error due to the size of antibody. Live-cell microtubule visualization can be achieved using fluorescently labeled taxanes,[8, 9] mEmerald-MAP4,[10] GFP-TPX,[11] protein-tags[12, 13] or graphene oxide guided peptide probe.[14] Such approaches are often time-consuming, as well as difficult to use in primary tissues and cells, thick tissues and multiple 3-dimentional-cell models. In addition to the arguments mentioned above, the small Stokes' shift of these fluorophores often results in added fluorescence signal from endogenous molecules, as well as unwanted background noise. Finally, with the exception of immune gold, there is not electron microscopy imaging probe available at present.

To this regard metal complexes comprising second/third row transition metals with high electron density and organelle specificity such as Ru(II), Ir(III) and Pt(II), and specific organic molecules allow metal-to-ligand charge transfer (MLCT) emission with high quantum yield and large Stokes' shifts.[15] The organic ligands can be designed to target molecules such as DNA[16] and bovine serum albumin (BSA)[17] and switch MLCT on only upon binding creating the so called 'light switch' effect.[18] These features are particularly useful when the organic ligands are used as probes for super resolution optical microscopy imaging such as stimulated emission depletion (STED), structured illumination microscopy (SIM), and stochastic optical reconstruction microscopy (STORM). Metal complexes have higher photon stability, than organic fluorophores, a critical parameter for enabling super

resolution micrographs (3-D micrographs).[19, 20] Finally, in conjunction with the above mentioned characteristics, the high electron density of the second/third row transition metals Ru(II), Ir(III) and Pt(II) used in our proposed system enable the complexes to scatter strongly the electron beam used in transmission electron microscopy (TEM). This results in a significant increase of contrast of otherwise almost invisible organic and biological matter. This is pivotal for the use of metal complexes in both transmission electron microscopy (TEM) and correlative light electron microscopy (CLEM).

The combination of both super-resolution optical and transmission electron microscopy enables the visualization of contextual information with the labeling provided by the fluorescence markers. This overcomes the limitations of using only light microscopy.[21] Imaging microtubulin in cells with both phosphorescent and electron microscopy using metal complex has never been reported before to the best of our knowledge.

We recently have reported the synthesis and use of metal complexes for the imaging of DNA, RNA and other subcellular organelles.[16, 22, 23] Herein we report the synthesis of a novel cyclometalated iridium(III) complex (**Ir-Tub)** designed by mimicking tubulin-binding vinblastine.[24] This was achieved by introducing thiazole moieties to tune hydrogen binding, π-π interaction with amino acid residues between α/β-Tubulin active pockets.[25] Iridium (III) complex possesses the necessary high electron density to provide contrast under TEM,[26] as well as a noise-free signal and high stability under laser scanning microscopy due to its large Stokes shift (> 100 nm) and elevated photostability.

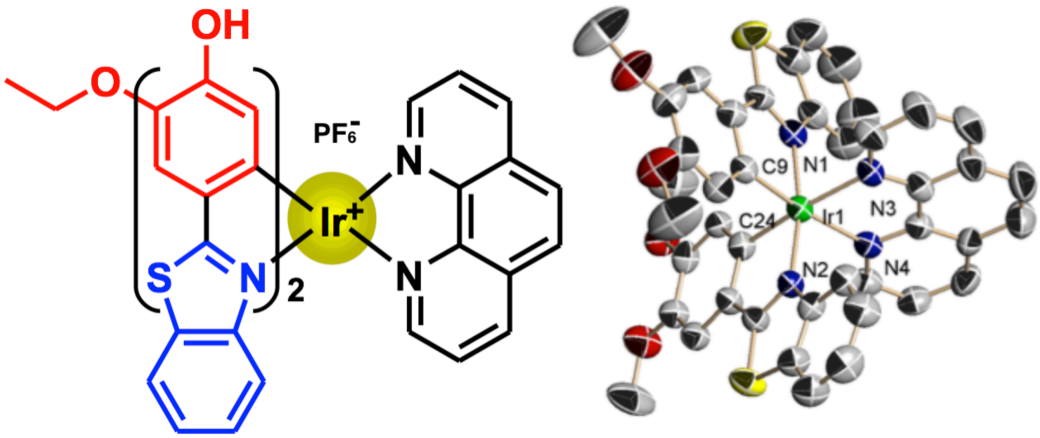

Scheme 1 Chemical Structure of **Ir-Tub** complex and its crystal structure, PF_6^- ion was omitted for clarity.

Results and Discussion:

The synthesis and characterization of the Ir(III) phenanthroline complex (**Ir-Tub, Scheme 1a**) is provided in the supporting information (**Scheme S1**, Supplementary **Fig. S1**) and the final product was crystallized (**Scheme 1b**). Due to the similarity of the molecular volume, aromaticity, solubility between **Ir-Tub** and vinblastine (**Fig. S2**), it is reasonable to assume that **Ir-Tub** complex may be sensitive to microtubules binding-site between α-β dimers, which in turn eventually causes photochemical change. Moreover, upon photo-excitation, **Ir-Tub** exhibited weak long-lived red luminescence (520-660 nm) and large Stock shift (>100 nm) which are in agreement with the crystal structure, UV-visible and TD-DFT calculation results (Fig. S3-4, Table S2). The above unique photon physical properties and its metal core provide possibility using **Ir-Tub** complex for optical and electronic microscopy, as well as extended STED super resolution techniques.

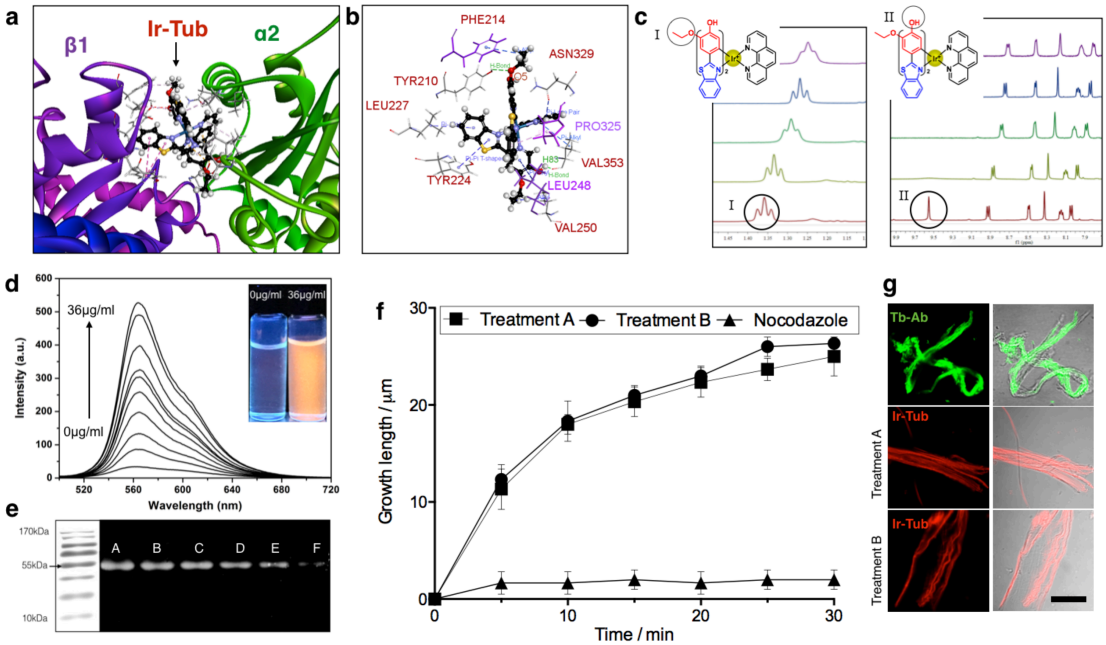

Fig. 1 *In vitro* assessment of the specificity between Ir-Tub complex and microtubules. (**a**) Computer modelling of Ir-Tub complex docking into two tubulin dimers (β-1, α-2). (**b**) Computer modelling of Ir-Tub complex detailed interaction with microtubules amino acid residues. (**c**) ^{1}H NMR titration experiments with increasing of tubulin protein concentration indicated the detailed binding site at Ir-Tub complex. (**d**) Fluorescence titration experiment using Ir-Tub complex with increasing levels of tubulin concentration (from 0 to 36 μg/ml, interval = 4 μg/ml). (**e**) SDS page image containing electrophoresed tubulin protein (~ 55 kDa), after staining with Ir-Tub complex. (**f**) *In vitro* growth of tubulin protein into microtubules under treatment-A, treatment-B, and 500 nM nocodazole as control, and (**g**) their correspondent fluorescent images, with acetyl K40 antibody immunofluorescence experiment confirmed the substance was microtubules. Scale Bar 20μm.

We firstly evaluated the affinity between **Ir-Tub** and microtubules *in vitro*. The specific recognition of **Ir-Tub** against tubulin protein (5J2T, PDB protein data base) was initially confirmed *via* molecular docking using the Discover Studio ligand fit Vina software (version 2016, The Biovia Co.).[27] The 5J2T PDB structure contains tubilin heterodimers and thus mimics the conformation of tubulin within microtubules whilst being tractable in terms of solubility and structural rigidity.[28] Therefore two tubulin dimers (α-1, β-1, α-2, β-2, Fig. 1a and Supplementary Fig S5) were firstly set as the minimal unit of receptor microtubules for **Ir-Tub**. As expected, vinblastine-binding site was replaced by **Ir-Tub** (Fig. 1a); the detailed interaction force including π-π interaction, π-alkyl interaction and hydrogen binding (Fig. 1b, Supplementary Fig S6 and Supplementary Movie S1) was clearly presented (Phe214, Asn329, Pro325, Val353, Leu248, Val250, Tyr224, Leu227 and Tyr210). It is notable that the

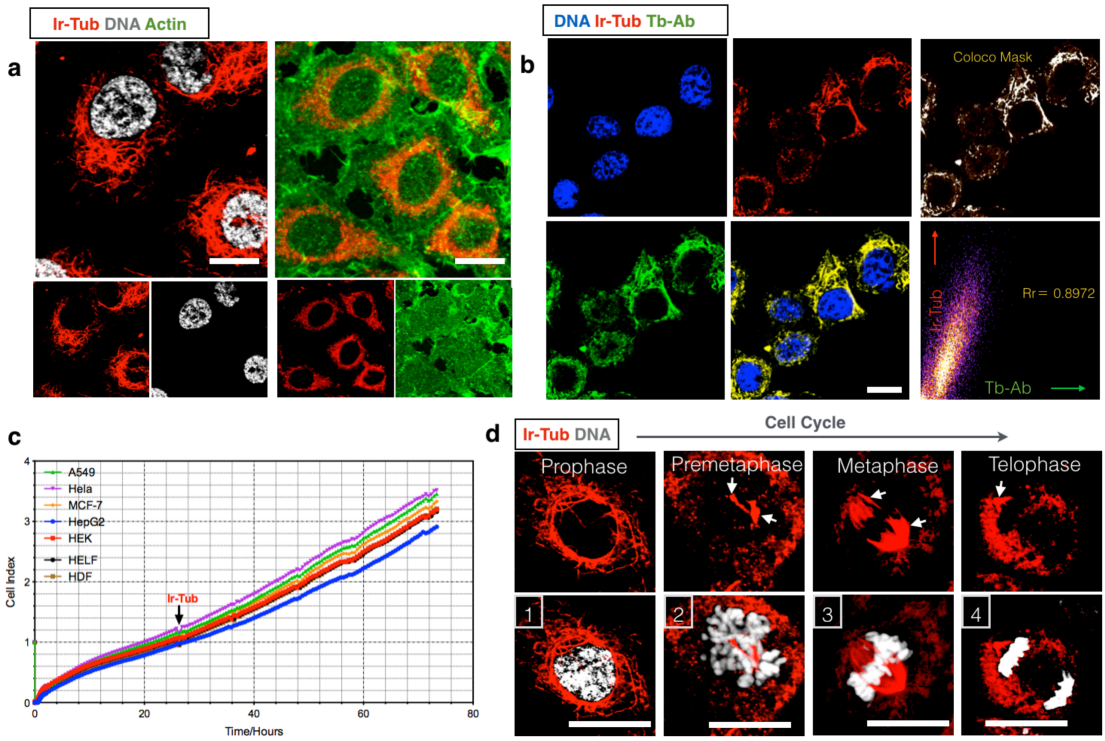

Fig. 2 *In cella* assessment of Ir-Tub complex interaction with microtubules. (**a)** Live HepG2 cells incubated with 5μM Ir-Tub complex for 30 min, and stained with NucRed (left) or Alexa488-phalloidin (right). (**b)** Live HepG2 cells incubated with Ir-Tub complex, then immunofluorescently labelled with acetyl K40 antibody for microtubules, and NucRed for DNA. Colocolization map and Pearson's coefficency showed high overlap degree between Ir-Tub complex and microtubules antibody. (**c)** Real-time monitoring of cell proliferation with initial 5μM Ir-Tub complex treatment on A549, HeLa, MCF-7, HepG2, HEK, HDF and HELF cells over 72 hours. (**d)** Magnified micrographs of synchronized living cells under different cell cycles (prophase, premetaphase, metaphase, and telophase) after 5 μM Ir-Tub complex incubation, while nuclear stained using NucRed. Scale Bar 10 μm.

calculated binding energy resulted in a docking score between **Ir-Tub** and tubulin protein ~10 folds higher than that of vinblastine (Supplementary Table S1).

We confirmed such a high affinity of the **Ir-Tub** complex against α-β tubulin protein, *via* ^{1}H NMR titration experiments. Purified tubulin protein was obtained using a classic method reported elsewhere.[29] Along the increase in tubulin protein concentration, the proton signals of the benzene ring were shifted up field and the H (II) of the ethoxy groups were also shifted up field, which might be explained by the C-H···π interactions between the β1-PHE214 and the ethoxy group of the **Ir-Tub** (Fig. 1c). The H (I) signal intensity of the phenolic hydroxyl group was sharply reduced after adding the tubulin protein (Fig. 1c), this possibly indicated that ethoxy group and phenolic hydroxyl groups provided the hydrogen binding sites for the tubulin protein (α2-VAL353). Moreover, the weak interactions between the C-O groups and PHE214, TYR210, VAL250 inhibited the twisting movement, which in turn hinders the non-radiative transition when the complex is bound to tubulin protein,

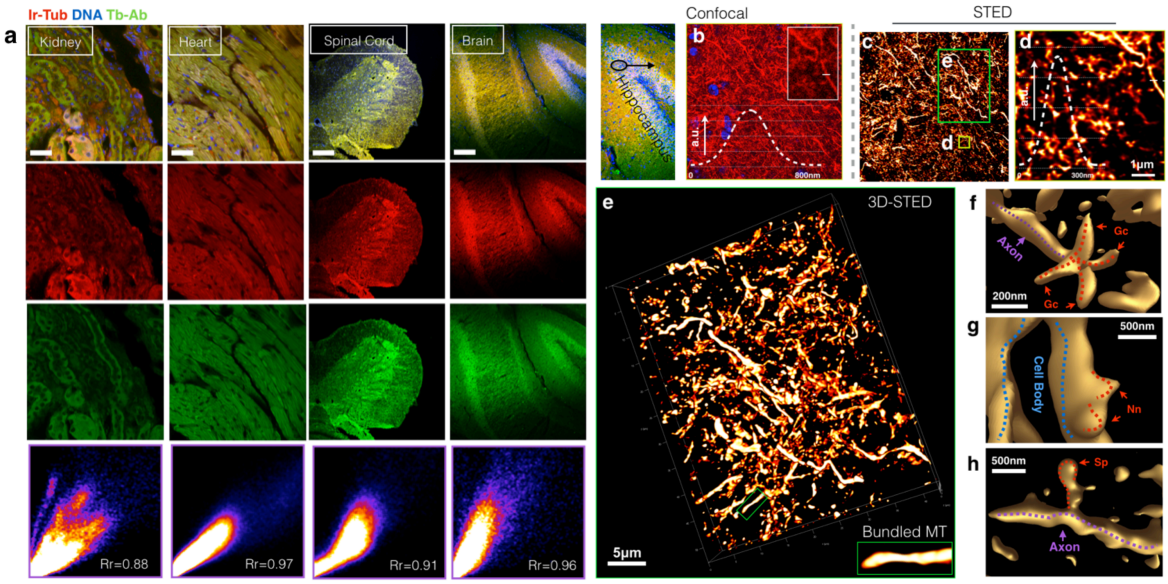

Fig. 3 *Ex Vivo* assessment of Ir-Tub complex at tissue level and its STED application using brain sections. (**a)** Fresh kidney, heart, spinal cord, and brain sections incubated with 5μM Ir-Tub complex for 30 min, then immunofluorescently labelled with acetyl K40 antibody for microtubules, and NucRed for DNA. The colocolization profile and calculated Pearson's coefficency indicated high degree of overlapping between Ir-Tub and microtubules antibody. Scale Bar= 50μm. (**b)** Confocal micrograph of selected region from brain hippocampus and its magnified image. Insert: The average signal intensity from the line profiles. (**c)** STED micrograph of the same region and its (**d)** magnified STED image. Insert: The average signal intensity from the line profiles. (**e)** Magnified 3D-STED image from selected regions from (**c**); Insert: the heavily bundled microtubules. 3D-STED indicated the ultrastructure of neuronal (**f)** growth cone (Gc), (**g)** new neurite (Nn), and (**h)** spine (Sp) ultrastructure with unprecedented resolution. The Purple dashed line displayed the axon in (**f**) and (**h**), and the blue dash line highlighted the neuronal cell body in (**g**).

showing ongoing decreased intensity as the tubulin protein contents dropped. Both experimental and computational results indicated that **Ir-Tub** complex does insert into microtubules, and its emission is enhanced due to multiple interactions with active amino acid residue sites.

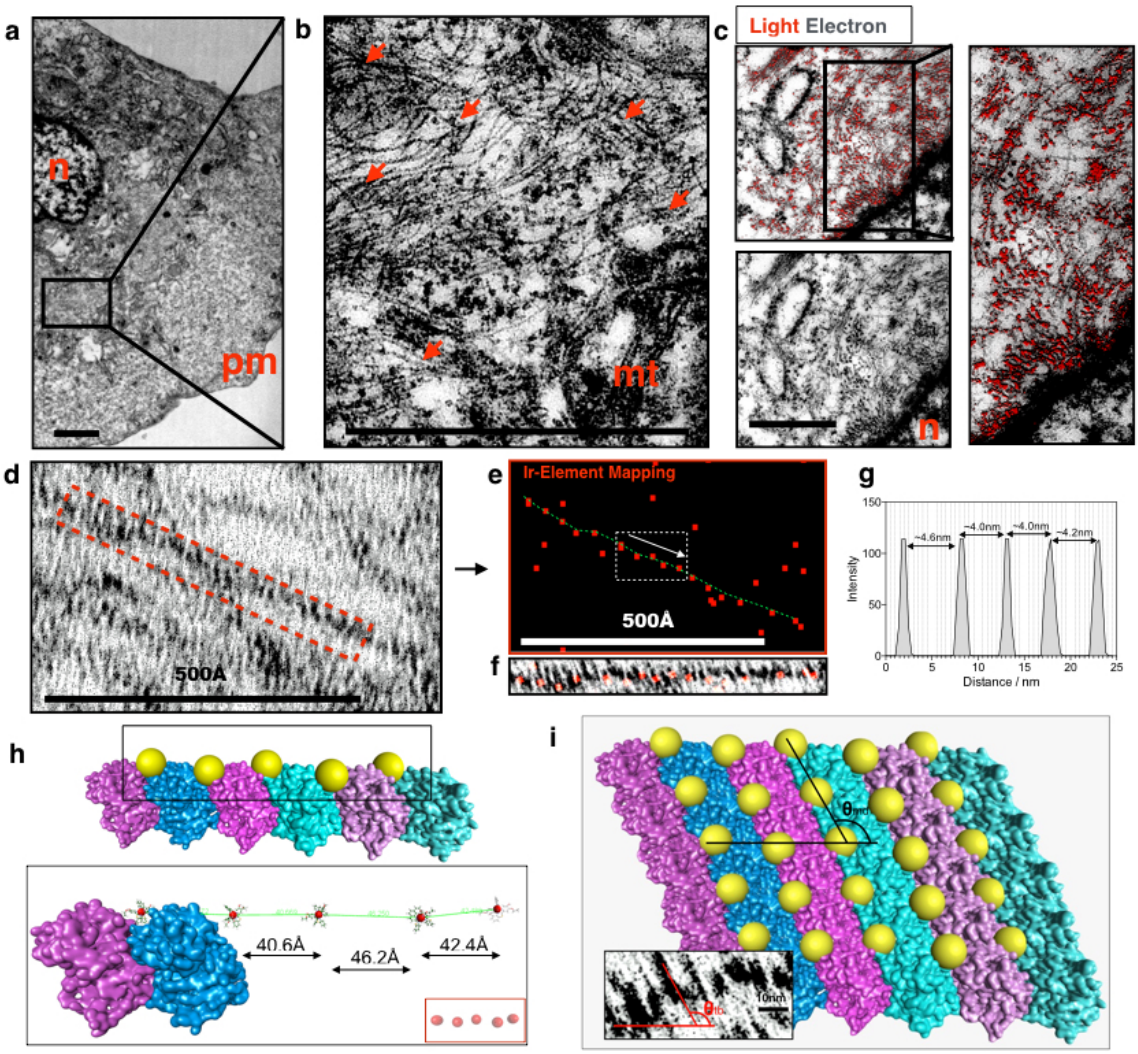

Fig. 4 TEM evaluation of Ir-Tub treated cells and its chemical mapping. (**a)** TEM image from an ultra-thin section of HepG2 cells pretreated with Ir-Tub,and membrane EM agent osmium tetroxide (OsO_4). (**b**) Magnified image from selected region clearly indicated Ir-Tub labeled microtubules, while OsO_4 stained mitochondria (**mt**), nucleus (**n**) and plasma membrane (pm). Further magnified image of a microtubule (**c**) Correlative light-electron microscopy evaluation of ultra-thin sections indicated the overlapped fluorescent and electronic signal. (**d** and **e**) Correlated Iridium mapping achieved in EF-TEM mode with superimposed image of the microtubule, (**f**) displaying how Ir-Tub complexes intercalate within microtubules stripes. (**g)** Distance measurement of neighboured Iridium elements, and (**h)** the comparison with the measured distance from thecomputational molecular model. (**i)** Angle measurement of neighboured microtubules stripes with its horizontal line as polar coordinate system (θ_{tb} = 68 °), and similar measurement from polymerized microtubule model (θ_{md} = 68 °).

dependent entry mechanisms regulates **Ir-Tub** uptake (Supplementary Fig. S12). Co-staining with the nuclear dye Nuc-red indicated very little signal overlap with **Ir-Tub**. As actin is the other predominate content for the cytoskeleton, further co-staining experiment using fluorescently labelled phalloidin and actin-binding was undertaken. No signal overlap between **Ir-Tub** and phalloidin was observed by confocal microscopy, suggesting that **Ir-Tub** does not bind to actin microfilaments and is tubulin-specific. **Ir-Tub** labeling works on live cells as well as on pre-fixed cells (Supplementary Fig. S10) were also presented. This allowed us to further prove tubulin selectivity by immunofluorescence using tubulin antibody (acetyl K40). The overlapping signal between **Ir-Tub** and tubulin antibody acetyl K40, as well as processed colocolization mask and Pearson's coefficient (Rr = 0.8972) strongly suggested that the subcellular target of **Ir-Tub** is indeed the microtubule protein. In order to confirm **Ir-Tub** does not inhibit polymerization of tubulin protein in live cells for an extended incubation period, cell proliferation experiments were performed using immortalized cancerous cells (A549, HeLa, MCF-7, HepG2 and HEK) as well as primary normal cells human dermal fibroblasts (HDF) and human embryo liver fibroblasts (HELF). These results showed that even at the optimal concentration for imaging, **Ir-Tub** had little influence in cells growth over 72 hours (i.e. 3 days), thus offering the possibility to monitor microtubules in living system over extended periods.

Centrosomes are mostly made of microtubules and act as fulcrum for chromosomes travelling to the two daughter cells during mitosis. We therefore tested the use of **Ir-Tub** for monitoring microtubules during mitosis. HepG2 cells were synchronized using nocadazole and thymidine.[33] Cells at (G0) G1-S (97.43 %), (G0) G1-S (47.78 %) co-existed with G2-M (52.22 %) and G2-M (96.92 %) and this was confirmed by flow cytometry (FACS) (Supplementary Fig. S11). The cells were further incubated with **Ir-Tub** complex and their binding to Tublin allowed for imagining. The higher magnification micrographs of cells at prophase, prometaphase, metaphase and telophase were also successfully captured; DNA was co-stained using Nuc-Red (Fig. 2d and Supplementary Fig. S13). Fig. 2d shows that while the nuclear membrane breaks down and DNA chromatin assembles into chromosomes (Fig. 2d-1), **Ir-Tub** labeled microtubules further polymerized to mother/ daughter centriole (Fig. 2d-2). The signal of **Ir-Tub** appears to migrate to opposite poles of the cell with clear indication of mitotic spindles (Fig. 2d-3 and 2d-4). Since structural and numeric aberrations (excess of centrosomes) can be a common observation in human

tumors,[34] the ability of **Ir-Tub** to effectively monitor microtubules in a dynamic manner during mitosis provides an attractive feature for cancer biology investigations.

The capabilities of **Ir-Tub** to mark microtubules at tissue level and its utilization under stimulated emission depletion (STED) microscopy were also explored. Herein, fresh tissue slices sectioned from liver, heart, spinal cord and brain were incubated with **Ir-Tub** complex for 30min and treated for immunofluorescence using anti- tubulin acetyl K40 antibody. As showed in Fig. 3a, **Ir-Tub** complex tubulin labeling overlapped strongly with acetyl K40 antibody in all the sections (Rr_{liver} = 0.88, Rr_{heart} = 0.97, $Rr_{spinal\ cord}$ = 0.91 and Rr_{brain} = 0.96). In Fig3a the nucleus has been labeled using classic DAPI staining. In particular in the microtubules-rich brain tissue, **Ir-Tub** staining showed clearly elongated fibril structures throughout the hippocampus region clearly highlighting the neuronal network. In addition, in the spinal cord sections, giant motor neurons cell were also clearly marked by the **Ir-Tub** complex (Supplementary Fig. S14).

We expected **Ir-Tub** with iridium metal core to be considerably less sensitive to the high laser power associated with STED imagining. This allowed the possibility to create STED-3D micrographs of neuronal networks with high spatial resolution. Typically STED

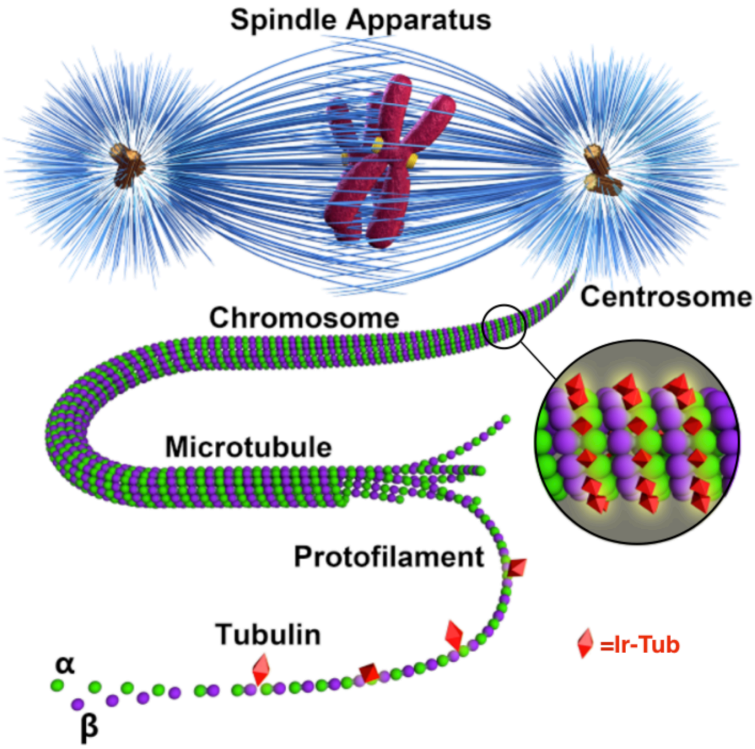

Fig. 5. Schematic representation of Ir-Tub complex internalized within α- (green) and β- (purple) tubulin and light up microtubules, within a mitotic spindle. The spindle apparatus, above microtubule structure, shows chromosomes (red), centrosomes (yellow) and microtubules (blue). Representation is not up to scale.

imaging requires the use of concentrated dyes with extreme high photon-stability consequently this may affect ultra-structure. It is known that microtubules are a major cytoskeletal component of neurons and they are critical for many fundamental cellular and developmental processes including neuronal differentiation migration and polarity.[35, 36] Metal complex **Ir-Tub** is ideal to provide bright and stable signal to construct precise neuron morphology particularly at three-dimensional level using STED imaging. As shown in Fig. 3b a region was selected from the hippocampus and imaged by confocal microscopy (resolution ~1μm). The super resolution micrograph was successfully obtained by STED and its resolution was significantly improved (Fig. 3c and 3d, resolution STED ~ 65 nm). Conventional confocal laser scanning microscopy shows the microtubules as very blurry and difficult to resolve, while the STED micrographs show microtubules as crisp fibril patterns with superb signal-to-noise ratio (Fig. 3c and 3d). Super-resolution micrographs based on 3D micrographs required the probe to possess outstanding photon resistance and brightness (> 150 Z-sections), which can be hardly achieved using commercial probes. The generated 3D-STED images (selected region from Fig. 3c, green frame) show very effectively the complex neuron microtubule network with < 50 nm resolution (Fig. 3e, Supplementary Fig. S15 and Supplementary Fig. S16). These include heavy bundled microtubules (Fig. 3e insert), growth cone (Gc, Fig. 3f), as well as nascent neurites (Nn, Fig. 3g) and spines (S, Fig. 3h). These observations clearly demonstrate the suitability of **Ir-Tub** as super-resolution imaging tool to study neuronal development and cargo transportation in the central nervous system.

We exploited the metal complexes to provide selective contrast for electron microscopy (EM).[16, 26] This was achieved by pretreating cells with **Ir-Tub,** sectioning them into 80 nm thick sections and imaging them by TEM. The membrane staining agent osmium tetroxide (OsO_4) for TEM was also applied post-fixation. The magnified TEM images from Fig. 4a show microtubules (tb) with fibril patterns (Fig. 4b), only in the cells treated with **Ir-Tub** as well as intracellular membrane morphology stained by OsO_4 including mitochondria (mt) (Fig. 4b), endocytotic caveolae (c) (Supplementary Fig. S17) or vesicles (v) and multi-vesicular body (MVB) (Supplementary Fig. S18). In comparison, cells solely treated with OsO_4 displayed a stained and resolved membrane but microtubule structures were not resolved in the TEM image (Supplementary Fig. S19). We also performed correlated light-electron microscopy (CLEM)[37] that images the ultra-thin sections sequentially under confocal microscopy (airyscan model) and scanning-transmission electron microscopy

(STEM). As shown in Fig. 4c, the MT network is both visible under EM and confocal imaging confirming the **Ir-Tub** affinity toward tubulin and showing its suitability for CLEM imaging. To further prove that the **Ir-Tub** is actually associated with the microtubules we also imaged the cell section using energy-filtered transmission electron microscopy (EF-TEM) in order to perform elemental analysis and thus fine structure imaging. In EF-TEM mode, chemical mapping was achieved by selecting electrons that have lost a specific amount of energy from inelastic scattering. In the case of inner shell ionization, the energy loss is characteristic of the element the electron interacted with in the specimen. In the present study this element was iridium, thus iridium O shell maps were acquired. The 3-window technique was employed (supporting information). In this technique three energy filters were selected to acquire three images, two before the specific energy loss edge for Iridium, to acquire the background, and one after, to acquire the intensity of the signal. The three images were computed to extract a map of Ir within the specimen. As shown in Fig. 4d, the iridium elemental map matches the tubular structure. The Iridium signal distribution pattern clearly overlapped with the microtubule stripes' signal (Fig.4e and 4f). Interestingly, the distance measurement along the elemental tubular structure (spacing ~ 40 Å – 46 Å, Fig.4g) coincided well with the values obtained from computer molecular model level (spacing ~40.6 Å -46.2 Å, Fig.4h). Notably, the measured angle (θ_{tb}=68°) between parallel microtubule stripes and their horizontal line (as polar coordinate system) from EF-TEM images showed perfect match with the angle obtained from the polymerized microtubule model (θ_{md}=68°) (Fig.4i). The above results strongly suggested that **Ir-Tub** complex could be effectively internalized within intracellular microtubules and indeed capable of acting as a multi-function probe under optical (Confocal and STED) and electron microscopy (TEM, STEM and EFTEM).

Conclusion:

In summary we have designed and synthesized an Iridium (III) complex **Ir-Tub** that is capable of binding to β-tubulin active pockets. The MLCT emission of the **Ir-Tub** complex 'switched on' upon tubulin binding with high specificity and sensitivity *in vitro* was observed. Further *in cella* studies firstly demonstrated that such probe not only enables microtubules tagging and monitoring of several cell phases during mitosis, but also shows minimal interference for cell proliferation over days. In particular, it is indicated that microtubules could be clearly observed using **Ir-Tub** at *ex vivo* tissue level, and further

STED micrographs displayed excellent signal-to-noise ratio. The iridium complex proposed by this study could indeed be used as an essential tool to further understand microtubule dynamics in living system, as well as a potential targeting vector for therapeutic purposes.

Acknowledgments

This work was supported by a grant for the National Natural Science Foundation of China (21602003, 51432001, 51672002, 51772002 and 21501001). G.B thank the support from Anhui 'Distinguished Foreign Expert' Programme, the EPSRC (EP/N010906/1) and Jeol for sponsoring LR-P salary and funding the Electron microscopy centre, DENSsolutions for sponsoring CDP studentship and The EPSRC (EP/N026322/1) for sponsoring his Fellowship. X.T thank Anhui Provincial Natural Science Foundation of China (1708085MC68), and Anhui University Doctor Startup Fund (J01001962), Anhui Provincial Returnees Innovation and Entrepreneurship key support program. We appreciated Ms Linda Liang and Mr Sheng Long from ZEISS Microscopy Customer Centre (Shanghai, China) to perform CLEM experiment. We also thank Leica (China) for STED assistance and data analysis.

Author Contribution

X. T., G.B., Z.Z and Y.T design the project. R. Z., Q. Z and Y.T design and synthesised the complex. R. Z., Q. Z and Z.Z. did all the characterization and data analysis. X.T., R. S., and M. Z. performed the cell and tissue florescent work including confocal and STED. Q.W. performed TEM sample preparation and sectioning. B.C. performed CLEM experiment and related data analysis. C. D. P., L.R.P and G.B performed the EF-TEM and analysis the data. X. T., Z.Z and G.B. wrote the paper.

Reference:

1. Zheng, Y., Wong, M.L., Alberts, B. & Mitchison, T. Nucleation of microtubule assembly by a gamma-tubulin-containing ring complex. *Nature* **378**, 578-583 (1995).
2. Fletcher, D.A. & Mullins, R.D. Cell mechanics and the cytoskeleton. *Nature* **463**, 485-492 (2010).
3. Canton, I. & Battaglia, G. Endocytosis at the nanoscale. *Chemical Society Reviews* **41**, 2718-2739 (2012).

4. Sharp, D.J., Rogers, G.C. & Scholey, J.M. Microtubule motors in mitosis. *Nature* **407**, 41-47 (2000).
5. Jordan, M.A. & Wilson, L. Microtubules as a target for anticancer drugs. *Nature Reviews Cancer* **4**, 253 (2004).
6. Bates, M., Huang, B., Dempsey, G.T. & Zhuang, X. Multicolor super-resolution imaging with photo-switchable fluorescent probes. *Science* **317**, 1749-1753 (2007).
7. Fernandez-Suarez, M. & Ting, A.Y. Fluorescent probes for super-resolution imaging in living cells. *Nat Rev Mol Cell Biol* **9**, 929-943 (2008).
8. Lukinavicius, G. et al. Fluorogenic probes for live-cell imaging of the cytoskeleton. *Nat Meth* **11**, 731-733 (2014).
9. Lukinavicius, G. et al. Fluorescent dyes and probes for super-resolution microscopy of microtubules and tracheoles in living cells and tissues. *Chemical Science* **9**, 3324-3334 (2018).
10. Planchon, T.A. et al. Rapid three-dimensional isotropic imaging of living cells using Bessel beam plane illumination. *Nat Meth* **8**, 417-423 (2011).
11. Wittmann, T., Wilm, M., Karsenti, E. & Vernos, I. TPX2, A novel xenopus MAP involved in spindle pole organization. *J Cell Biol* **149**, 1405-1418 (2000).
12. Lukinavičius, G. et al. A near-infrared fluorophore for live-cell super-resolution microscopy of cellular proteins. *Nature Chemistry* **5**, 132 (2013).
13. Lee, H.-l.D. et al. Superresolution Imaging of Targeted Proteins in Fixed and Living Cells Using Photoactivatable Organic Fluorophores. *Journal of the American Chemical Society* **132**, 15099-15101 (2010).
14. Li, Q.-R. et al. Graphene oxide-enhanced cytoskeleton imaging and mitosis tracking. *Chemical Communications* **53**, 3373-3376 (2017).
15. Lo, K.K.-W. Luminescent rhenium (I) and iridium (III) polypyridine complexes as biological probes, imaging reagents, and photocytotoxic agents. *Accounts of chemical research* **48**, 2985-2995 (2015).
16. Gill, M.R. et al. A ruthenium (II) polypyridyl complex for direct imaging of DNA structure in living cells. *Nature chemistry* **1**, 662-667 (2009).
17. Wu, P. et al. Cyclometalated Platinum(II) Complexes as Highly Sensitive Luminescent Switch-On Probes for Practical Application in Protein Staining and Cell Imaging. *Chemistry – A European Journal* **15**, 3652-3656 (2009).
18. Gill, M.R. & Thomas, J.A. Ruthenium(II) polypyridyl complexes and DNA--from structural probes to cellular imaging and therapeutics. *Chem Soc Rev* **41**, 3179-3192 (2012).
19. Sreedharan, S. et al. Multimodal Super-resolution Optical Microscopy Using a Transition-Metal-Based Probe Provides Unprecedented Capabilities for Imaging Both Nuclear Chromatin and Mitochondria. *Journal of the American Chemical Society* **139**, 15907-15913 (2017).
20. Byrne, A., Burke, C.S. & Keyes, T.E. Precision targeted ruthenium(ii) luminophores; highly effective probes for cell imaging by stimulated emission depletion (STED) microscopy. *Chem Sci* **7**, 6551-6562 (2016).
21. Liss, V., Barlag, B., Nietschke, M. & Hensel, M. Self-labelling enzymes as universal tags for fluorescence microscopy, super-resolution microscopy and electron microscopy. *Scientific Reports* **5**, 17740 (2015).
22. Tian, X. et al. Probe for simultaneous membrane and nucleus labeling in living cells and in vivo bioimaging using a two-photon absorption water-soluble Zn(ii)

terpyridine complex with a reduced [small pi]-conjugation system. *Chemical Science* **8**, 142-149 (2017).
23. Tian, X. et al. Halides tuning the subcellular-targeting in two-photon emissive complexes via different uptake mechanisms. *Chemical Communications* **53**, 7941-7944 (2017).
24. Gigant, B. et al. Structural basis for the regulation of tubulin by vinblastine. *Nature* **435**, 519-522 (2005).
25. Waight, A.B. et al. Structural Basis of Microtubule Destabilization by Potent Auristatin Anti-Mitotics. *PLOS ONE* **11**, e0160890 (2016).
26. Tian, X. et al. Localization matters: a nuclear targeting two-photon absorption iridium complex in photodynamic therapy. *Chemical Communications* **53**, 3303-3306 (2017).
27. Biovia, D.S. Discovery Studio Modeling Environment Release 2017. *Dassault Systèmes, San Diego, CA* (2016).
28. Yang, J. et al. Pironetin reacts covalently with cysteine-316 of α-tubulin to destabilize microtubule. *Nature Communications* **7**, 12103 (2016).
29. Shelanski, M.L., Gaskin, F. & Cantor, C.R. Microtubule Assembly in the Absence of Added Nucleotides. *Proceedings of the National Academy of Sciences* **70**, 765-768 (1973).
30. Vicidomini, G., Moneron, G., Eggeling, C., Rittweger, E. & Hell, S.W. STED with wavelengths closer to the emission maximum. *Opt. Express* **20**, 5225 (2012).
31. Castoldi, M. & Popov, A.V. Purification of brain tubulin through two cycles of polymerization–depolymerization in a high-molarity buffer. *Protein expression and purification* **32**, 83-88 (2003).
32. Vasquez, R.J., Howell, B., Yvon, A., Wadsworth, P. & Cassimeris, L. Nanomolar concentrations of nocodazole alter microtubule dynamic instability in vivo and in vitro. *Molecular biology of the cell* **8**, 973-985 (1997).
33. Zieve, G.W., Turnbull, D., Mullins, J.M. & McIntosh, J.R. Production of large numbers of mitotic mammalian cells by use of the reversible microtubule inhibitor Nocodazole: Nocodazole accumulated mitotic cells. *Experimental Cell Research* **126**, 397-405 (1980).
34. Nigg, E.A. Centrosome aberrations: cause or consequence of cancer progression? *Nature Reviews Cancer* **2**, 815 (2002).
35. Kapitein, L.C. & Hoogenraad, C.C. Building the Neuronal Microtubule Cytoskeleton. *Neuron* **87**, 492-506 (2015).
36. Arimura, N. & Kaibuchi, K. Neuronal polarity: from extracellular signals to intracellular mechanisms. *Nature Reviews Neuroscience* **8**, 194 (2007).
37. Peddie, C.J. et al. Correlative and integrated light and electron microscopy of in-resin GFP fluorescence, used to localise diacylglycerol in mammalian cells. *Ultramicroscopy* **143**, 3-14 (2014).